Applied Physics A (2025) 131:300
https://doi.org/10.1007/s00339-025-08431-z

Crystallographic and optical properties of ZnO nanoparticles prepared by two different methods

Betty Flores[1] · Maribel Guzman[2] · Oscar Chumpitaz[3] · Santiago Flores[3] · Andres Rodriguez[4] · Jose E. Herrera[4]

Received: 22 August 2024 / Accepted: 9 March 2025 / Published online: 21 March 2025

Abstract

This research presents the synthesis of nanoparticles of ZnO (Nps-ZnO) obtained by two methods: chemical precipitation (method 1) and combustion in solution (method 2). The effect of each method on the crystallographic properties of Nps-ZnO is studied. The Nps-ZnO obtained present, according to EDS analysis, an atomic Zn: O ratio of 0.95 and 1.36 when two methods were used respectively. The formation of Nps-ZnO with Wurtzite-type hexagonal arrangement is confirmed with XRD analysis. XRD results show there is not a big difference between the lattice parameters and interplanar spacing for the samples obtained by the two synthesis methods. However, the Nps-ZnO obtained by chemical precipitation show higher values of dislocation density (1.780×10^{-3}) nm^{-2} than those obtained by combustion in solution (0.152×10^{-3}) nm^{-2}. A similar behavior is observed with the micro-strain values (2.137×10^{-3}-6.388×10^{-3}) and (1.170×10^{-3}-1.971×10^{-3}), respectively. TEM images show nanoparticles with mean diameters between 17.2 ± 10.8 nm and 73.4 ± 6.0 nm when the method of chemical precipitation and combustion in solution were applied, respectively. Larger and semi-square nanoparticles are formed with the combustion in solution method is applied. Size of Nps-ZnO estimated from TEM images analysis, Debye-Scherer's formula and Rietveld refinement are highly inter-correlated. Finally, the Nps-ZnO presented a narrow bandgap of 3.19 eV and 3.16 eV, a value lower than that of the bulk material (3.7 eV). No drastic change in bandgap is observed for samples synthesized with two different methods.

Keywords Bandgap · Chemical precipitation · Combustion in solution · Dislocation density · Micro-strain · Nanoparticles · Zinc oxide

1 Introduction

Semiconductors have driven the last century of technological advancement [1]. Without them, the operation of various electronic devices would not be possible. Zinc oxide (ZnO) is one of the most important metal oxides due to its relative abundance, and its wide and direct band gap (~3.37 eV). The band gap of ZnO can be tuned either by decreasing the size of the crystallites [2-6] or by using a different synthesis method to obtain the oxide [7].

On the other hand, ZnO can not only have a potential application in electronics but in other industries such as agriculture, cosmetics, environment, food packaging, gas sensors, medicine and recently the construction industry [8, 9]. Depending on the application intended for Nps-ZnO, the synthesis method must be appropriate to guarantee that the suitable material will be obtained and take full advantage of the characteristics desired. For example, the crystallographic properties of Nps-ZnO can affect its mechanical behavior [10, 11]. Then, if we want to use Nps-ZnO as a material for smart food packaging, we must ensure that its mechanical properties of elongation and flexibility are as required [12-14].

Some studies have reported the influence of the synthesis parameters in a single method on the crystallographic

✉ Maribel Guzman
mguzman@pucp.edu.pe

1 Sciences Department, Pontifical Catholic University of Peru, Avenida Universitaria 1801, Lima, Peru

2 Engineering Department, Pontifical Catholic University of Peru, Avenida Universitaria 1801, Lima, Peru

3 Institute of Corrosion and Protection (ICP- PUCP), Pontifical Catholic University of Peru, Avenida Universitaria 1801, Lima, Peru

4 Department of Chemical and Biochemical Engineering, Western University, London, ON N6A 5B9, Canada

properties. Such is the case of Al-Gaashani et al. [15] who have evaluated the influence of the morphology of ZnO nanostructures obtained by microwave synthesis on the texture coefficients. However, few studies referring to the comparison of crystallographic properties of ZnO nanostructures prepared by various methods have been reported. Hasany et al. [16] studied and compared crystallographic properties of ZnO nanostructures synthesized by routes involving sol–gel and precipitation techniques. While Bhardwaj et al. [17] and Abushad et al. [18] compared the crystallographic properties such as lattice strain, lattice stress and unit cell volume of ZnO nanostructures obtained by sol-gel and hydrothermal methods, respectively. While the influence of three synthesis methods: combustion, coprecipitation and hydrothermal method were evaluated by Rajput et al. [19].

The literature has reported on a wide variety of synthesis methods ranging from reactions in aqueous medium to gas phase processes [20-22]. The result of each procedure will be to obtain Nps-ZnO with different sizes, shapes, crystallographic parameters, among others. However, it is still a challenge to control its crystal structure if the synthesis parameters are not adjusted appropriately [23]. Among all methods to obtain ZnO nanostructures [24-29], the two simplest methods as precipitation [6, 30-40] and combustion in solution [31-45] were chosen in order to compare their synthesis parameters in shape, size and crystallographic properties of the nanoparticles obtained. Considering that the precipitation method in an aqueous medium is carried out in two stages (nucleation and continuous growth of nuclei) [46] and the combustion in solution method is an extremely fast reaction [47-49], we want to know if there is any relationship between the method used and the average size, shape and lattice parameters of the samples obtained.

The present work reports the preliminary results of the synthesis and characterization of Nps-ZnO obtained by two synthesis methods and their influence on the size and shape. Likewise, the dislocation density, microstrain and bandgap of Nps-ZnO are also evaluated in order to confirm the potential of this material for applications as additives in the construction industry and optoelectronic devices, respectively.

2 Experimental

2.1 Materials and apparatus

Glycine, $NH_2CH_2CO_2H$ (≥ 99%), Potassium nitrate, KNO_3 (≥ 98%); Sodium hydroxide, NaOH (≥ 99%) and Zinc nitrate, $Zn(NO_3)_2.6H_2O$ (≥ 98%) were purchased from Sigma-Aldrich (Darmstadt, Germany). Commercial zinc oxide particles (≥ 98%) were used as a reference material. All chemicals were of analytical purity and used as received without further purification. Milli-Q water (18 MΩ cm), obtained from a purification system (Millipore, Darmstadt, Germany), was used. A commercial sample of ZnO particles was provided by Sigma-Aldrich (Darmstadt, Germany).

2.2 Chemical precipitation

Precipitation was carried out at 60ºC by adding a sodium hydroxide solution (NaOH; 0.4 M) dropwise to a container containing a homogeneous mixture of zinc nitrate ($Zn(NO_3)_2$; 20 mM) and potassium nitrate (KNO_3; 10 mM) in a K^+/Zn^{2+} ratio of 1:1 [50]. The pH of the reaction was kept constant at 11. After two hours, the nanoparticles obtained were separated by filtration (Whatman®: 0.02 µm pore size and 47 mm diameter). To eliminate remaining ions, the product was washed twice with deionized water. The samples obtained were dried in an oven at 60 °C for a period of 24 h. Then the samples were placed in a desiccator.

2.3 Combustion in solution

For the solution combustion synthesis, 5 g of zinc nitrate and 0.3 g of glycine (as fuel and oxidant) were dissolved in 20 ml of water. A viscous-looking solution was obtained under continuous magnetic stirring [41, 51]. The mixture was taken to a closed furnace preheated to 500 °C so that, after approximately 2 min, combustion takes place. Almost instantly, the mixture inside the crucible ignited due to combustion, producing a release of large quantities of gases (CO_2, N_2 and H_2O); which leave a porous product (nanocrystalline ZnO) at the bottom of the crucible. After the combustion is completed, the crucible is cooled to room temperature. The product obtained is removed from the crucible and ground in an agate mortar.

3 Results and discussion

Figure 1 presents the EDS spectra and percentage element compositions (inset table) of the Nps-ZnO obtained by chemical precipitation, combustion in solution and a commercial sample. Well-defined K and L emission peaks can be observed corresponding to zinc (K_a=8.630 keV and L_a = 1.012 keV) and oxygen (K_a =0.525 keV). In addition to the C emission peak (K_a = 0.277 keV) typical of the sample holder tape, no other peaks related to any contaminant are observed. Khan et al. [4], Kumar et al. [52], Anbuvannan et al. [53], and Manikandan et al. [54] reported similar EDS results for ZnO nanoparticles. The elemental compositions obtained through EDS correspond to a Zn: O atomic ratio of 0.95 and 1.36 for the ZnO nanoparticles obtained by precipitation method [31, 33, 55, 56] and combustion in solution

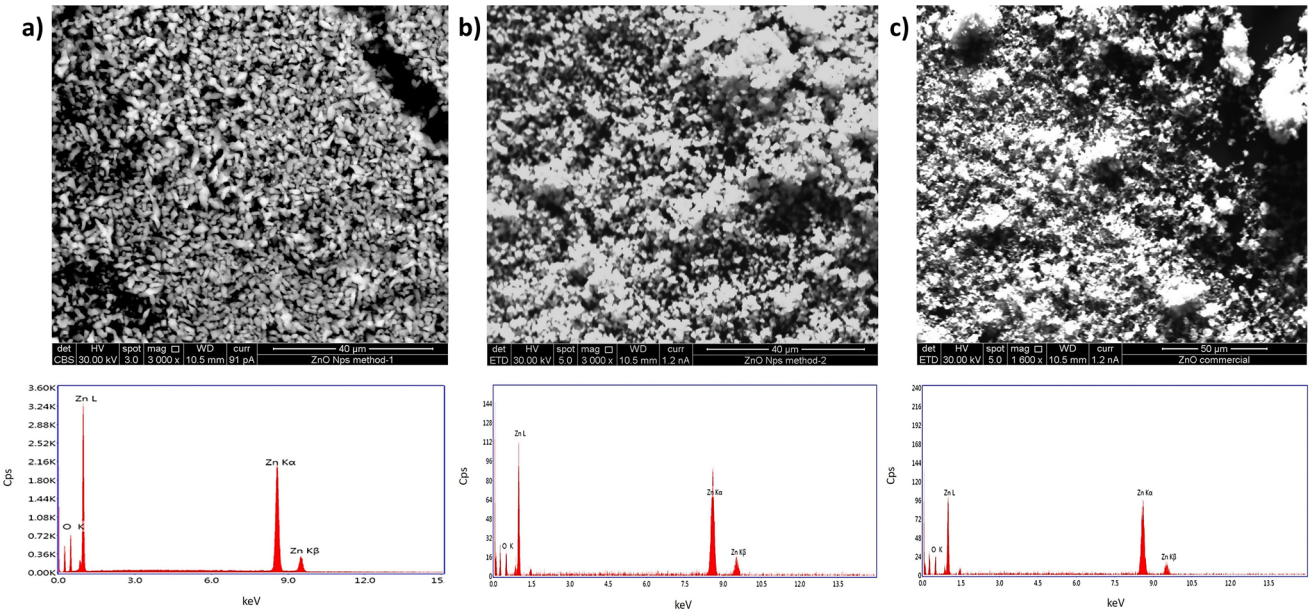

Fig. 1 EDS spectra of ZnO nanoparticles (**a**) obtained by chemical precipitation. (**b**) obtained by combustion in solution. (**c**) commercial

Table 1 The atomic percentage ratio of Zn and O in ZnO Nps prepared by using different methods

Method	Atomic (%) percentage of the elements.		
	Zn	O	Zn/O
Chemical precipitation	48.69	51.31	0.95
Combustion in solution	57.57	42.43	1.36
Commercial*	54.51	45.49	1.20

*Reference material

[45], respectively; while the commercial sample reported a value of 1.20 [2, 6]. Table 1 summarizes the atomic percentage of elements and the Zn/O ratio of each sample based on the EDS results.

The FTIR spectra of the three ZnO samples is presented in Fig. 2. The band around 3245 cm^{-1} indicate the presence of O-H bonds due to absorption of atmospheric humidity and the peak at 2347 cm^{-1} correspond to the C=O bond due to traces of environmental carbon dioxide solubilized during the reaction or adhered to the surface of the nanoparticles [57-59]. The peaks at 434 and 489 cm^{-1} corresponds to the stretching vibrations of the Zn-O bond [5, 30, 57, 60-66]. Then, the FTIR spectra confirm the formation of ZnO.

The XRD spectra of all samples are presented in Fig. 3. The family of planes indexed according to JCPD card no. 36-1451 for wurtzite-type zinc oxide confirm the formation of the hexagonal zinc oxide phase with a space group

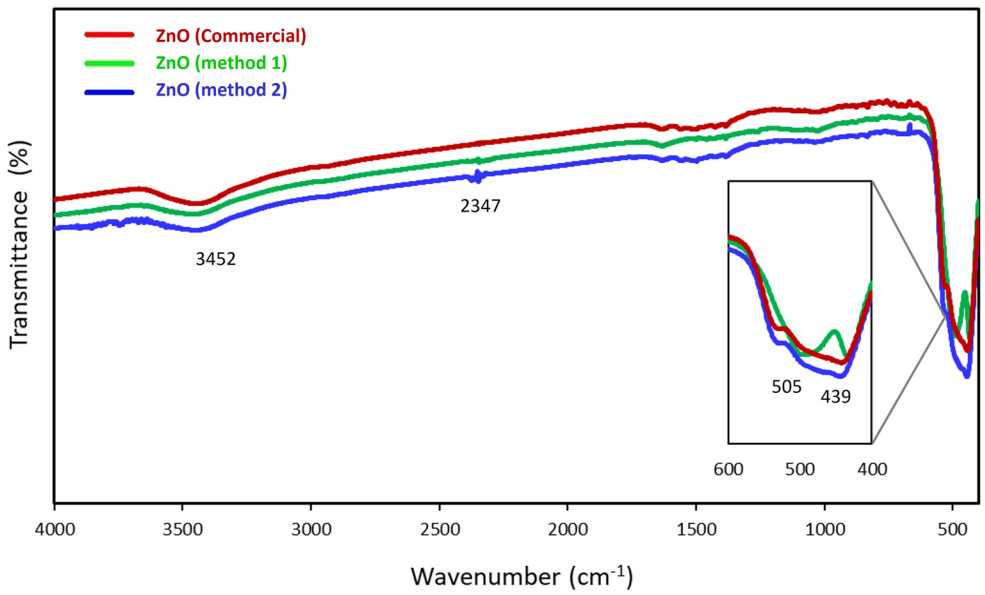

Fig. 2 FTIR spectra of Nps-ZnO samples prepared by chemical precipitation, combustion in solution and commercial sample.

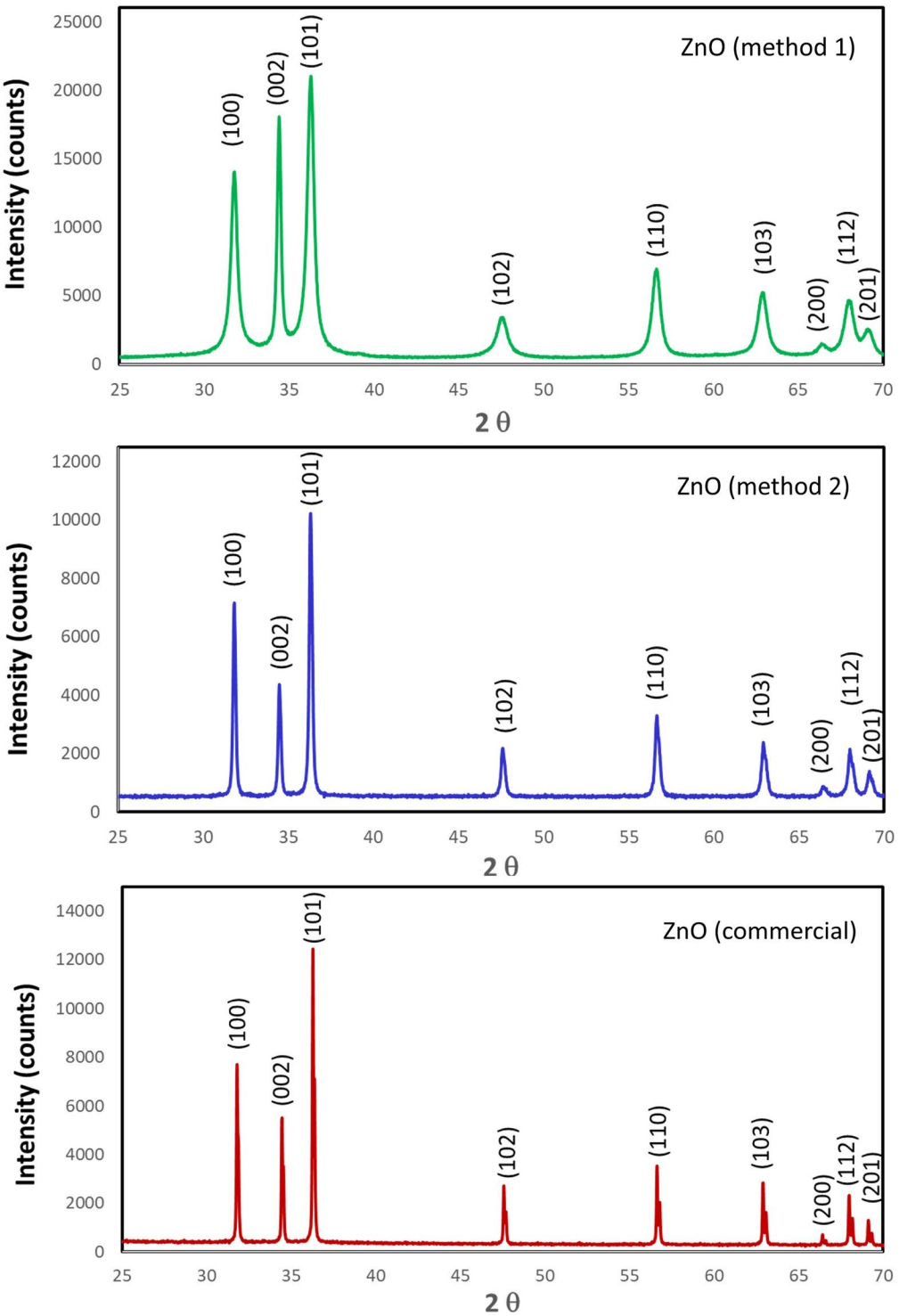

Fig. 3 X-ray diffraction patterns of Nps-ZnO samples prepared by chemical precipitation, combustion in solution and commercial sample

$P6_3mc$ [2, 4, 30, 67, 68]. No other diffraction peaks appear in the XRD patterns. Figure 3 shows nine well-defined diffraction peaks. The (101) peak located between 36º and 37º is the most intense, which would indicate that the Nps-ZnO obtained by both methods present a predominant crystallographic orientation along the (101) plane. Rietveld refinement on the X-ray data (XRD) of Nps-ZnO by selecting the space group ($P6_3mc$) was performed using Topas software by Brucker [69]. The lattice parameters and atomic sites used for the Rietveld refinement were $a = 3.2490$ (Å),

$c = 5.2060$ (Å), $Zn_{(x)} = O_{(x)} = 0.3333$ and $Zn_{(y)} = O_{(y)} = 0.6667$, respectively. Figure 4 shows the observed, measured and fitted XRD profiles of the Nps-ZnO samples after the final refinement cycle [70]. It can observe that the measured and fitted profiles match without major difference. The formation of wurtzite-type hexagonal ZnO nanocrystals without any other phase has been confirmed by refinement.

The Rietveld refinement R-factors such as R_B (Bragg factor), R_{exp} (expected factor), R_F (crystallographic factor), R_p (profile factor) and R_{wp} (weighted profile factor), along with the lattice parameters are summarized in the Table 2. The value of goodness of fit value (χ^2) is determined with R_{exp} and R_{wp} factors [71, 72, 73]. The χ^2 around 1.0 for the commercial ZnO sample ($\chi^2 = 1.17$) and sample obtained by combustion in solution ($\chi^2 = 1.54$) [74, 75] reveal high

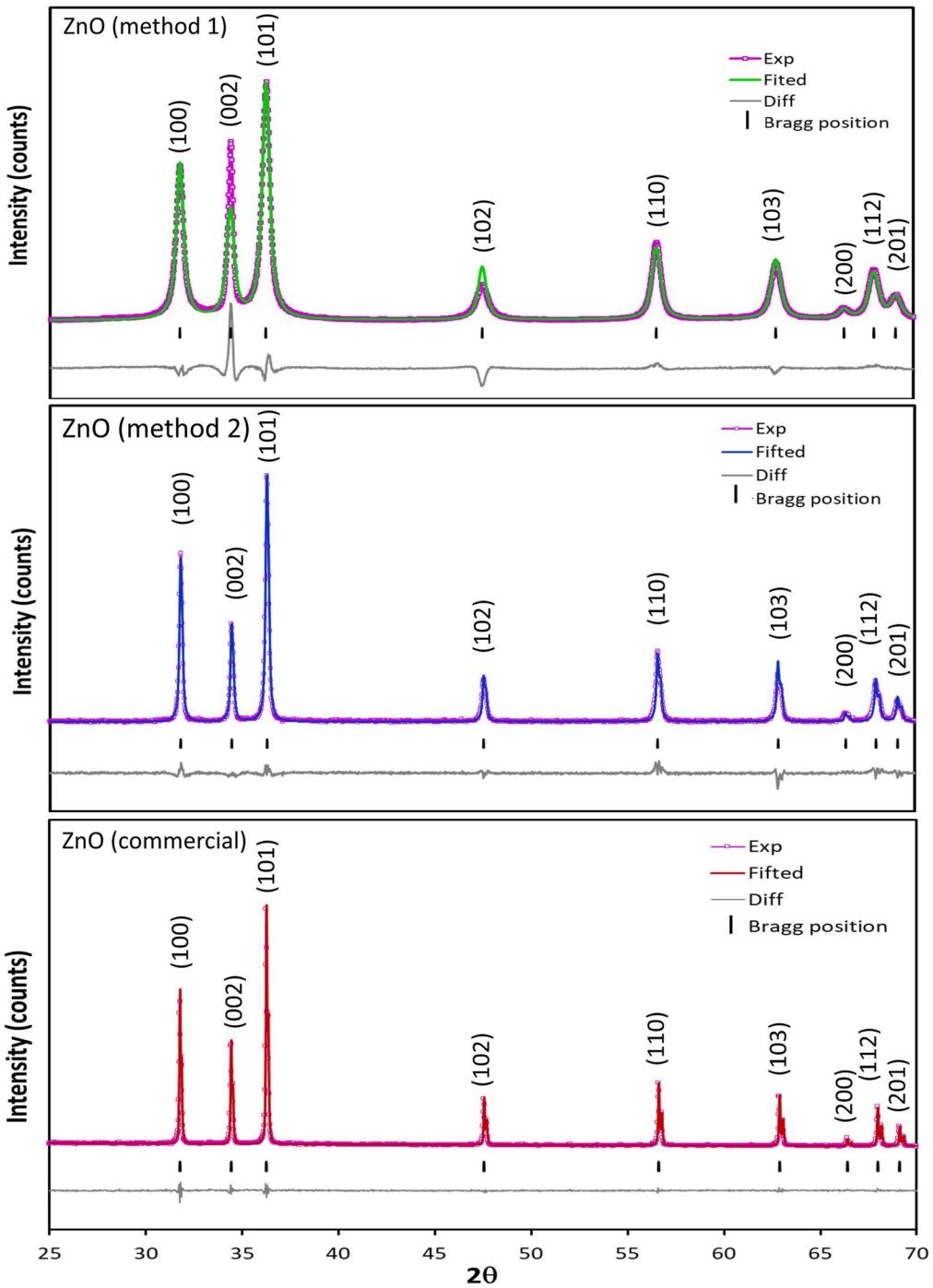

Fig. 4 Experimental and simulated diffraction pattern with Rietveld refinement of Nps-ZnO obtained by chemical precipitation (method 1), combustion in solution (method 2) and reference sample (commercial)

Table 2 Rietveld refined structural parameters of ZnO nanoparticles synthesized with two different methods

	Standard[(1)]	Chemical precipitation	Combustion in solution	Commercial[(2)]
$a \pm \sigma$ (Å)	3.24900	3.25080 ± 0.00518	3.24987 ± 0.00287	3.24983 ± 0.00183
$c \pm \sigma$ (Å)	5.20600	5.21105 ± 0.00750	5.20665 ± 0.00365	5.20641 ± 0.00241
c/*a* ratio	1.60234	1.60300	1.60211	1.60206
V (Å^3)	47.620	47.691	47.623	47.620
R-factors and χ^2	---	R_B: 3.030	R_B: 2.603	R_B: 0.573
	---	R_{exp}: 2.47	R_{exp}: 3.72	R_{exp}: 4.70
	---	R_p: 6.75	R_p: 4.29	R_p: 4.34
	---	R_{wp}: 10.33	R_{wp}: 5.73	R_{wp}: 5.48
	---	χ^2: 4.18	χ^2: 1.54	χ^2: 1.17
Strain	---	0.3474698	0.2629193	0.06266225
Positional parameter, u	0.37983	0.37972	0.37987	0.37987
Zn–O Bond length (nm)	19.77387	19.78742	19.77826	19.77781
Density, d (nm^{-2}) x 1000	---	1.780	0.152	0.152
Crystallite size Rietveld refinement, D (nm)	---	23.7	81.1	258.4
Crystallite size Debye-Scherrer, D ± σ, (nm)	---	23.5 ± 6.9	55.1 ± 6.7	128.1 ± 5.7

(1) JCPD (no. 36-1451); (2) Reference material

quality of the fit. Refined structural parameters of hexagonal Nps-ZnO as lattice parameters [33, 39, 76, 77, 78], positional parameter of the structure [79, 80], volume of the unit cell [33, 39, 81], the length of the Zn–O bond [79, 80], dislocation density [82-84] are presented in Table 2. It can be observed that there is no great variation in the values of lattice parameters, volume of the unit cell, positional parameter of the structure and length of the Zn-O bond of the Nps-ZnO prepared by the two different methods. The slight deviation of these parameters with reference to an ideal wurtzite crystal is probably due to the lattice stability and ionicity [85]. It is observed that the Nps-ZnO prepared by chemical precipitation show a higher density of dislocations than the other samples. Then there is a greater number of crystal defects in the crystal lattice.

In Fig. 5 show different microstructural parameters plotted against crystallite size. After refinement, it is observed that the lattice parameters *a* and *c* increase with the decrease in the size of the crystallites, which is reflected by the expansion of the lattice volume. The lattice strain has been found to increase with reducing crystallite size. This is explained because by reducing the size of the crystallites the surface atoms can lead to a stress field that leads to an increasing lattice distortion on the surface [86, 87].

Others crystallographic parameters such as interplanar distance [33, 88], texture coefficient [33, 78, 89] and micro strain [77, 90, 91, 92] were determined from the XRD data (Fig. 6). The results are presented in Table 3. According to the results of the texture coefficient (TC > 1) [93], the crystallites of the Nps-ZnO obtained by combustion in solution are preferably oriented in the (100), (200) and (201) planes while those obtained by precipitation will be oriented in the (002) and (200) directions. Finally, the Nps-ZnO obtained by chemical precipitation has a greater degree of distortion of the crystal lattice [94], since high micro-strain values are observed.

The estimated size of ZnO nanocrystal using the Debye-Scherrer formula [33, 39, 76, 95] and Rietveld refinement [96, 97] are presented in Table 2. The calculated nanocrystal size by Debye-Scherrer were 23.5 ± 6.9 nm, 55.1 ± 6.7 nm and 128.1 ± 5.7 nm for samples obtained by precipitation method, combustion in solution and the commercial sample, respectively. With the precipitation method, smaller nanocrystals are obtained than with the combustion in solution. A contrary result was previously reported by Krobthong et al. [98]. This could be explained by the stages involved in each process. The combustion in solution method is carried out in a single step [99] while through chemical precipitation a competition of the nucleation and growth of nucleus by diffusion phenomena occurs in parallel [51, 100, 101]. In fact, combustion in solution is an extremely rapid process (a few seconds to a few minutes) in which a rapid exothermic reaction produces nanometer-sized powders [102, 103]; while the precipitation process can take longer to carry out (from several minutes to hours).

Figure 7 shows typical TEM micrographs obtained for each sample. The precipitated sample presents a wide range of shapes for the nanoparticles, some of which are hemispherical, while the sample obtained by combustion in solution presents almost square-shaped nanoparticles. We attribute this difference in morphology to the synthesis method used. In fact, the formation of nanoparticles by precipitation probably takes place through two parallel processes: nucleation and continuous growth of nuclei. The chemical reactions that occur in the precipitation method are as follows [51, 100]:undefined

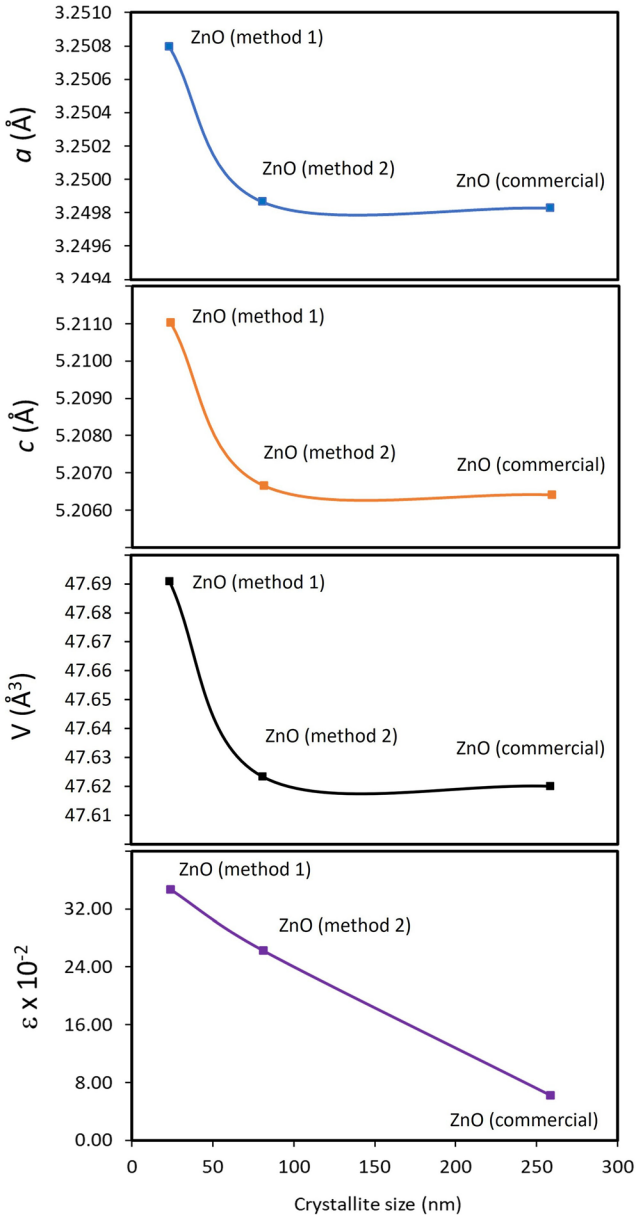

Fig. 5 Variation of the microstructural parameters with crystallite size

$$Zn^{2+}_{(aq)} + 2\,(OH)^{-}_{(aq)} \leftrightarrows Zn(OH)_{2(s)} \quad K = 3.3\,\mathrm{x}10^{16} \tag{1}$$

{\rm{x}}{10^{16}} \cr}]]>

$$Zn(OH)_{2(s)} + 2\,(OH)^{-}_{(aq)} \leftrightarrows Zn\,(OH)^{2-}_{4(aq)} \quad K = 4.6\,\mathrm{x}10^{17} \tag{2}$$

undefined{\rm{x}}{10^{17}} \cr}]]>

$$Zn\,(OH)^{2-}_{4(aq)} \leftrightarrows ZnO_{(s)} + 2H_2O_{(l)} + 2OH^{-}_{(aq)} \quad K = 1.6\,\mathrm{x}10^{2} \tag{3}$$

undefined{\rm{x}}{10^2} \cr}]]>

Then depending on the working conditions, mainly pH and temperature, Eqs. (1), (2) and (3) can be reversible. If the processes are reversible, then we can assume that the particles can dissolve again and those ions can join other particles, then larger particles are obtained, with a broader size distribution. At the beginning of the precipitation, when the thermodynamic threshold for saturation occurs, ZnO nuclei will be formed. These ZnO nuclei will give way to the growth process to form semi spherical ZnO nano particles. For Nps-ZnO obtained by combustion in solution, the nanoparticles are obtained through the following reaction [99]:

$$Zn^{2+}_{(aq)} + 2NO^{-}_{3(aq)} + 2CH_2(NH_2)COOH_{(aq)} + 2O_{2(g)} \xrightarrow{\Delta} ZnO_{(s)} + 4CO_{2(g)} + 5H_2O_{(g)} + 2N_{2(g)} \tag{4}$$

Since the reaction is extremely fast, in this case the growth process takes place in the solid residue from the combustion [47]. So, slightly bigger-sized particles ought to be attributed to the aggregation or overlapping of small particle [104]. Also, unlike the chemical precipitation method, the solution combustion method is carried out in a single stage according to reaction (4). If we compare the two synthesis methods, it is observed that the precipitation method produces smaller nanoparticles (17.2 nm ± 10.8 nm) with a wider size distribution. While for combustion synthesis, the nanoparticles obtained are slightly larger (73.4 nm ± 6.0 nm) but present a narrower size distribution, implying that this method allows for a better particle size control. As the combustion in solution is an irreversible process, there is no possibility that the particles will dissolve again and grow more, therefore there is better size control during synthesis.

The direct bandgap energy (Egap) of Nps-ZnO was calculated using information from the UV-Vis absorption spectra (Fig. 8a) according the following expression:

$$(\alpha h\nu)^{(1/p)} = A(h\nu - E_{gap}) \tag{5}$$

where a is the absorption coefficient, h is Planck's constant, ν the frequency of the incident photons, p is the transition probability ($p = 1/2$), A is a constant and E_{gap} is the optical bandgap [2, 3, 60, 105]. By plotting the absorption coefficient multiplied by the energy of a photon all squared $(\alpha h\nu)^2$ vs. the photon energy we obtain an exponential plot (Fig. 8b). By extending the tangent towards the abscissa and intercepting this axis, we will obtain the value of the Energy of the bandgap (Fig. 8b). The direct band gap of the ZnO nanoparticles obtained by precipitation was 3.19 eV [2]. It can be seen that it is a value lower than 3.37 eV (theoretical bandgap) [106]. This bandgap value determined

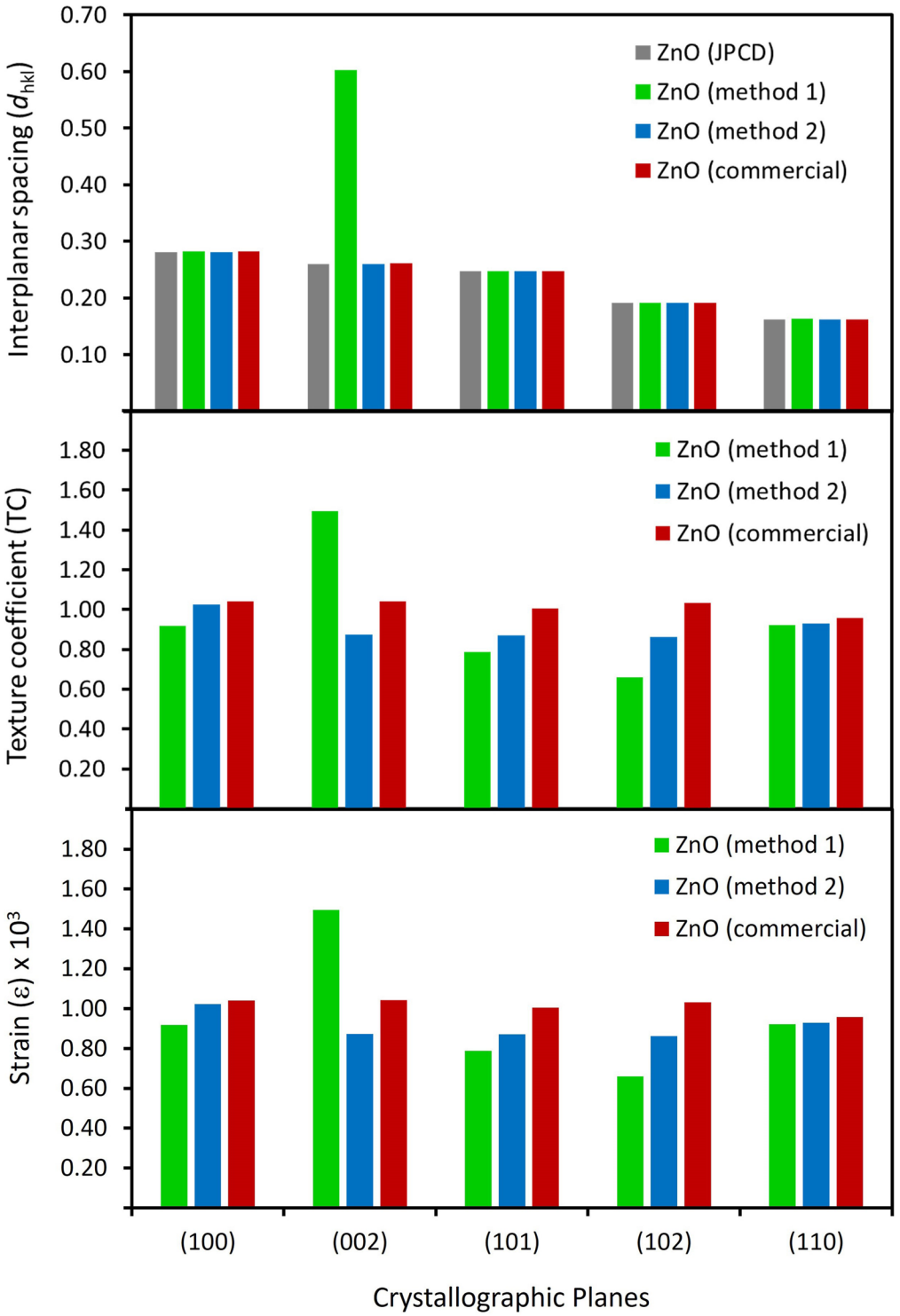

Fig. 6 Interplanar spacing, texture coefficient and micro-strain of Nps-ZnO samples

experimentally is close to that reported by Josun et al. [107], Ba-Abbad et al. [2] and Parra et al. [6] for Nps-ZnO with mean diameters of 16 nm, 20 nm and 44 nm, respectively. In the case of the sample obtained by the combustion in solution, the experimental bandgap was 3.16 eV. Similar value was previously reported by Lopes de Almeida et al. [5] for ZnO nanoparticles with smaller crystallite sizes (20 nm). Slightly smaller bandgap values were reported by Vasei et al. [42] for ZnO nanoparticles between 18 nm and 36 nm.

Table 3 The interplanar spacing of ZnO nanoparticles synthesized with two different methods

hkl	Interplanar spacing, d_{hkl} (Å)			
	Method 1	Method 2	Reference	JPCD [71]
(100)	0.2816 ± 0.0012	0.2812 ± 0.0029	0.2814 ± 0.0050	0.281
(002)	0.2605 ± 0.0012	0.2601 ± 0.0043	0.2603 ± 0.0051	0.260
(101)	0.2478 ± 0.0011	0.2474 ± 0.0075	0.2476 ± 0.0003	0.247
(102)	0.1912 ± 0.0006	0.1910 ± 0.0010	0.1911 ± 0.0016	0.191
(110)	0.1625 ± 0.0004	0.1624 ± 0.0012	0.1625 ± 0.0005	0.162
(103)	0.1478 ± 0.0004	0.1477 ± 0.0010	0.1477 ± 0.0010	0.147
(200)	0.1407 ± 0.0002	0.1407 ± 0.0039	0.1407 ± 0.0010	0.140
(112)	0.1379 ± 0.0003	0.1378 ± 0.0014	0.1379 ± 0.0011	0.137
(201)	0.1359 ± 0.0002	0.1358 ± 0.0002	0.1359 ± 0.0008	0.135

Method 1: Chemical precipitation; Method 2: Combustion in solution; Reference: Commercial sample

The bandgap of a commercial sample was also determined as a reference (E_{gap} = 3.22 eV) [108].

It is observed that the bandgap does not depend entirely on the size of the crystallite, therefore the increase in bandgap with the decrease in its size due to the effect of optical confinement cannot be completely established [2, 5, 6, 105] (Table 5). Likewise, it is observed that the bandgap is not strongly affected by the average size of the nanoparticles and the synthesis methods of Nps-ZnO [3, 4]. However, a slight decrease in bandgap can be seen with the morphology [109] and the synthesis methods of the synthesized Nps-ZnO [105] (Table 5).

Previous studies have shown that the morphology of ZnO nanostructures can influence their bandgap [110, 111]. These changes in the Egap would confirm that the crystal grain size and the crystal growth facets lead to the effective band gap of the nanostructured ZnO smaller than its total value of 3.37 eV [26, 110, 111, 112, 113]. Indeed, the E_{gap} variation could be explained by defects related to the surface of the nanoparticles and/or species adsorbed during the synthesis [60, 69]. Indeed, the luminescence properties of nanometer-sized zinc oxide (ZnO) colloids are highly dependent on their surface properties [109].

4 Conclusions

In summary, the method of production influences the morphology, the size distribution, average size and the crystallite size of Nps-ZnO; obtaining smaller nanoparticles with chemical precipitation method is used. Rietveld refinement of the XRD patterns of ZnO nanocrystals allowed detailed information on their microstructure. Rietveld refined analysis of XRD confirms that Nps-ZnO with hexagonal structure and space group $P6_3mc$ were obtained. Some crystallographic parameters, such as dislocation density and microstrain values, are influenced by the synthesis method used; while the interplanar distance, lattice parameters, and structure positional parameter are not drastically affected when the two different synthesis methods proposed in this study were used. Likewise, depending on the texture coefficient,

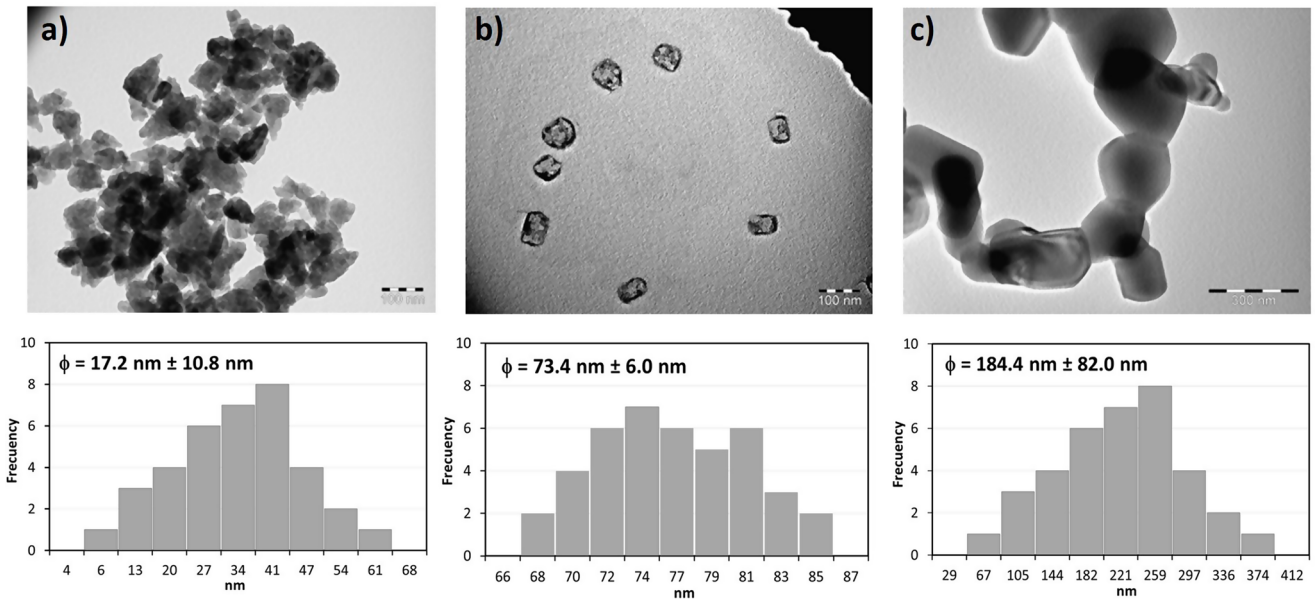

Fig. 7 TEM images and particle size distribution of Nps-ZnO samples

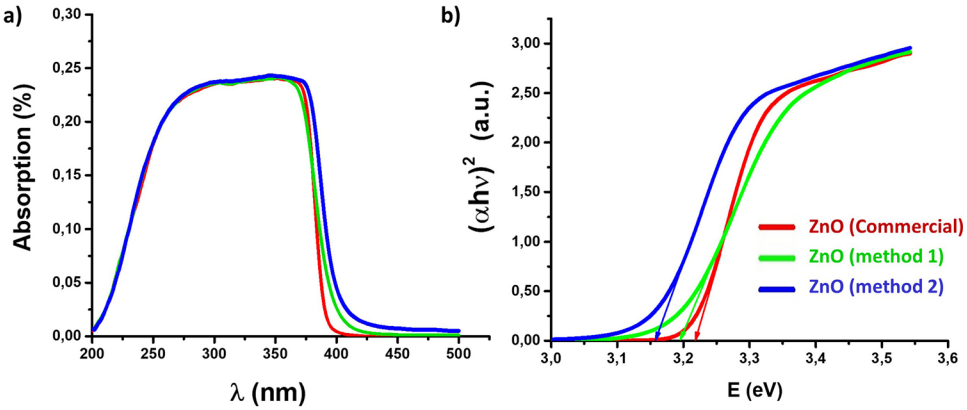

Fig. 8 **a**) UV-Vis spectra. **b**) and direct band gap of Nps-ZnO samples

Table 4 The texture coefficient and strain of ZnO nanoparticles synthesized with two different methods

hkl	Texture coefficient (TC)			Strain (e) x 1000		
	Method 1	Method 2	Reference	Method 1	Method 2	Reference
(100)	0.9189 ± 0.0110	1.0240 ± 0.0761	1.0411 ± 0.0651	6.3877 ± 0.0261	1.9711 ± 0.0020	0.9318 ± 0.0017
(002)	1.4956 ± 0.4321	0.8725 ± 0.0030	1.0423 ± 0.0806	3.2259 ± 0.0153	1.7501 ± 0.0029	0.9476 ± 0.0019
(101)	0.7875 ± 0.0847	0.8711 ± 0.0510	1.0047 ± 0.0253	5.2109 ± 0.0233	1.8203 ± 0.0056	0.8684 ± 0.0001
(102)	0.6601 ± 0.1424	0.8615 ± 0.0795	1.0325 ± 0.0962	5.3648 ± 0.0156	1.5773 ± 0.0008	0.6993 ± 0.0006
(110)	0.9211 ± 0.0422	0.9295 ± 0.0571	0.9579 ± 0.0407	4.0133 ± 0.0088	1.4590 ± 0.0010	0.5538 ± 0.0002
(103)	0.8016 ± 0.0015	0.7715 ± 0.0025	0.8662 ± 0.0183	3.4951 ± 0.0098	1.4156 ± 0.0010	0.5403 ± 0.0005
(200)	1.5573 ± 0.0258	1.7567 ± 0.0627	1.2262 ± 0.3821	2.3563 ± 0.0018	1.4075 ± 0.0022	0.5564 ± 0.0002
(112)	0.8764 ± 0.1391	0.8577 ± 0.0794	0.8571 ± 0.0304	2.7512 ± 0.0052	1.2045 ± 0.0012	0.4544 ± 0.0004
(201)	0.9815 ± 0.0355	1.0556 ± 0.3226	0.9719 ± 0.1115	2.1367 ± 0.0039	1.1703 ± 0.0002	0.4780 ± 0.0003

Method 1: Chemical precipitation; Method 2: Combustion in solution; Reference: Commercial sample

Table 5 Mean diameter, crystallite size and direct band gap energy of ZnO nanoparticles synthesized with two different methods

Method	Average Particles Size from TEM (nm)	Crystallite size (nm)		Experimental Band gap energy (eV)
		Debye-Scherrer	Rietveld refinement	
Chemical precipitation	17.2 ± 10.8	23.5 ± 6.9	23.7	3.19
Solution combustion synthesis	73.4 ± 6.0	55.1 ± 6.7	81.1	3.16
Commercial*	184.4 ± 82.0	128.1 ± 5.7	258.4	3.22

*Reference material

it is observed that the crystallographic orientations of the samples vary when precipitation or combustion in solution method is used. The orientation in the (001) plane of the sample obtained by chemical precipitation is evident. No significant difference in the bandgap energy was observed for any of the two prepared samples. In other words, there is no significant effect on the E_{gap} in both nanoparticles' samples obtained by precipitation (3.19 eV) and combustion in solution (3.16 eV). The crystallographic and optical properties of Nps-ZnO prepared by both methods confirm that this material can be used in optical applications. However, element doping tests will need to be performed to explore their influence on preparation methods.

Supplementary Information The online version contains supplementary material available at https://doi.org/10.1007/s00339-025-08431-z.

Acknowledgements M. Guzmán is very grateful to the Materials Characterization Center (CAM) of the PUCP and the 4MAT of the Université Libre de Bruxelles, Belgium for the facilities to carry out the XRD, SEM and TEM tests, respectively. This work was supported Pontifical Catholic University of Peru (GRANT: 017-2019); Canada Foundation of Innovation (CFI PROJECT NUMBER: 17025); and Global Affairs Canada Faculty Mobility for Partnership Building Program (FMBP-2022-GA-1-UWO).

Author contribution Betty Flores: Investigation. Maribel Guzman: Conceptualization, Methodology, Writing - original draft, Writing - review & editing. Oscar Chumpitaz: Methodology. Santiago Flores: Supervision, Resources. Andres Rodriguez: Formal analysis. Jose E. Herrera: Resources, Writing - review & editing.

Funding Open access funding provided by Pontificia Universidad Catolica del Peru.

Data availability Data will be made available on request.

Declarations

Competing interest The authors declare that they have no known competing financial interests or personal relationships that could have appeared to influence the work reported in this paper.

References

1. J. Orton, The First Hundred Years: From Faraday to Yesterday, Semiconductors and the Information Revolution, 1st EditionAcademic Press, Amsterdam, (2009), pp 31–56
2. M.M. Ba-Abbad, A.A.H. Kadhum, A.B. Mohamad, M.S. Takriff, K. Sopian, J. Alloys Compd. **550**, 63 (2013). https://doi.org/10.1016/j.jallcom.2012.09.076
3. L.K. Jangir, Y. Kumari, A. Kumar, M. Kumar, K. Awasthi, Mater. Chem. Front. **1**, 1413 (2017). https://doi.org/10.1039/C7QM00058H
4. M.M. Khan, N.H. Saadah, M.E. Khan, M.H. Harunsani, A.L. Tan, M.H. Cho, Mater. Sci. Semicond. Process. **91**, 194 (2019). https://doi.org/10.1016/j.mssp.2018.11.030
5. W. Lopes de Almeida, N.S. Ferreira, F.S. Rodembusch, V. Caldas de Sousa, Mater. Chem. Phys. **258**, 123926 (2021). https://doi.org/10.1016/j.matchemphys.2020.123926
6. M.R. Parra, F.Z. Haque, J. Mater. Res. Technol. **3**, 363 (2014). https://doi.org/10.1016/j.jmrt.2014.07.001
7. L.I. Ali, S.A. El-Molla, M.M. Ibrahim, H.R. Mahmoud, M.A. Naghmash, Opt. Mater. **58**, 484 (2016). https://doi.org/10.1016/j.optmat.2016.05.034
8. R. Garg, R. Garg, Mater. Today Proc. 43, 778 (2021) https://doi.org/10.1016/j.matpr.2020.06.168
9. M.A. Subhan, N. Neogi, K.P. Choudhury, Nanomanuf. **2**, 265 (2022). https://doi.org/10.3390/nanomanufacturing2040016
10. A.J. Desai, A. Ashock, V.V. Dabir et al., J. Mater. Sci: Mater. Electron. **34**, 1899 (2023). https://doi.org/10.1007/s10854-023-11292-y
11. R. Suntako, Adv. Mat. Res. **1044**, 23 (2014). https://doi.org/10.4028/www.scientific.net/AMR.1044-1045.23
12. S. Smaouia, I. Chérif, H.B. Hlima, M.U. Khan, M. Rebezov, M. Thiruvengadam, T. Sarkar, M.A. Shariati, J.M. Lorenzo, Food Packaging Shelf Life. **36**, 101045 (2023). https://doi.org/10.1016/j.fpsl.2023.101045
13. H. Helmiyati, Z.S. Zakiyah, I.F. Royani, D. Liftyawati, Polym. Test. **104**, 107412 (2021). https://doi.org/10.1016/j.polymertesting.2021.107412
14. K.K. Dash, P. Deka, S.P. Bangar, V. Chaudhary, M. Trif, A. Rusu, Polym. (Basel). **14**, 521 (2022). https://doi.org/10.3390/polym14030521
15. R. Al-Gaashani, S. Radiman, A.R. Daud, N. Tabet, Y. Al-Douri, Ceram. Int. **39**, 2283 (2013). https://doi.org/10.1016/j.ceramint.2012.08.075
16. S.F. Hasany, S. Hussain, S.M.U. Ali, W. Abdul-Kadhim, M. Amir, Micro Nano Lett. **15**, 972 (2020). https://doi.org/10.1049/mnl.2019.0795
17. R. Bhardwaj, A. Bharti, J.P. Singh, K.H. Chae, N. Goyal, S. Gautam, Heliyon. **4** (2018). https://doi.org/10.1016/j.heliyon.2018.e00594. e00594
18. M. Abushad, Z. Hassan, S. Naseem, S. Husain, W. Khan, AIP Conf. Proc. 2265, 030133 (2020) https://doi.org/10.1063/5.0017057
19. P. Rajput, P. Vashishtha, G. Gupta, K. Pathania, Mater. Today: Proc. 43, 3856 (2021) https://doi.org/10.1016/j.matpr.2020.12.1177
20. Z. Jiang, B. Liu, L. Yu, Y. Tong, M. Yan, R. Zhang, W. Han, Y. Hao, L. Shangguan, S. Zhang, W. Li, J. Alloys Compd. **956**, 170316 (2023). https://doi.org/10.1016/j.jallcom.2023.170316
21. C.B. Ong, L.Y. Ng, A.W. Mohammad, Renew. Sustain. Energy Rev. **81**, 536 (2018). https://doi.org/10.1016/j.rser.2017.08.020
22. A. Kołodziejczak-Radzimska, T. Jesionowski, Materials. **7**, 2833 (2014). https://doi.org/10.3390/ma7042833
23. D. Cao, S. Gong, X. Shu, D. Zhu, S. Liang, Nanoscale Res. Lett. **14**, 210 (2019). https://doi.org/10.1186/s11671-019-3038-3
24. N. Matinise, X.G. Fuku, K. Kaviyarasu, N. Mayedwa, M. Maaza, Appl. Surf. Sci. **406**, 339 (2017). https://doi.org/10.1016/j.apsusc.2017.01.219A
25. C. Janaki, E. Sailatha, S. Gunasekaran, S. Acta, A. Mol, Biomol. Spectrosc. **144**, 17 (2015). https://doi.org/10.1016/j.saa.2015.02.041
26. K.J. Rao, V. Kumaravel, I. Pownraj, K. Saha, T. Korumilli, S.K. Sadasivam, J. Clean. Prod. **380**, 135180 (2022). https://doi.org/10.1016/j.jclepro.2022.135180
27. D. Sharma, J. Rajput, B.S. Kaith, M. Kaur, S. Sharma, Thin Solid Films. **519**, 1224 (2010). https://doi.org/10.1016/j.tsf.2010.08.073
28. F.T. Thema, E. Manikandan, M.S. Dhlamini, M. Maaza, Mater. Lett. **161**, 124 (2015). https://doi.org/10.1016/j.matlet.2015.08.052
29. L.H. Zhao, R. Zhang, J. Zhang, S.Q. Sun, Cryst. Eng. Comm. **14**, 945 (2012). https://doi.org/10.1039/C1CE05621B
30. K. Pushpanathan, S. Sathya, M.J. Chithra, Mater. Manuf. Process. **27**, 1334 (2012). https://doi.org/10.1080/10426914.2012.700163
31. D.B. Bharti, A.V. Bharati, J. Lumin. **32**, 317 (2017). https://doi.org/10.1002/bio.3180
32. R.V. Gopal, S. Kamila, Appl. Nanosci. **7**, 75 (2017). https://doi.org/10.1002/bio.3180
33. M. Kahouli, A. Barhoumi, A. Bouzid, A. Al-Hajry, S. Guermazi, Superlattices Microstruct. **85**, 7 (2015). https://doi.org/10.1016/j.spmi.2015.05.007
34. E.A. Meulenkamp, J. Phys. Chem. B **102**, 5566 (1998). https://doi.org/10.1021/jp980730h
35. D. Raoufi, J. Lumin. **134**, 213 (2013). https://doi.org/10.1016/j.jlumin.2012.08.045
36. M. Gusattia, G.S. Barroso, C.E. Maduro, D.A. Ribeiro, J. de Almeida, R. Bohn, C. Cardoso, L. Abreu, H. Gracher, N. Cabral, Mater. Res. **14**, 264 (2011). https://doi.org/10.1590/S1516-14392011005000035
37. M. Ramani, S. Ponnusamy, C. Muthamizhchelvan, J. Cullen, S. Krishnamurthy, E. Marsili, Colloids Surf. B **105**, 24 (2013). https://doi.org/10.1016/j.colsurfb.2012.12.056
38. Z.M. Khoshhesab, M. Sarfaraz, M.A. Asadabad, Inorg. Metal-Org. Nano-Met Chem. **41**, 814 (2011). https://doi.org/10.1080/15533174.2011.591308

39. A. Sahai, N. Goswami, E. Physica, Low-Dimensi. Syst. Nanostruct. **58**, 130 (2014). https://doi.org/10.1016/j.physe.2013.12.009
40. B. Bekele, A. Degefa, F. Tesgera, L.T. Jule, R. Shanmugam, L.P. Dwarampudi, N. Nagaprasad, K. Ramasamy, J. Nanomater. 2021, 9210817 (2021) https://doi.org/10.1155/2021/9210817
41. S. Flores, O. Chumpitaz, Rev. de Metal. 55, e139 (2019) https://doi.org/10.3989/revmetalm.139
42. H.V. Vasei, S.M. Masoudpanah, M. Habibollahzadeh, Mater. Res. Bull. **125**, 110784 (2020). https://doi.org/10.1016/j.materresbull.2020.110784
43. V. Gowthambabu, A. Balamurugan, R.D. Bharathy, S. Satheeshkumar, S.S. Kanmani, Acta Part. A: Mol. Biomol. Spectrosc. **258**, 119857 (2021). https://doi.org/10.1016/j.saa.2021.119857
44. G. Manjunath, S. Pujari, D.R. Patil, S. Mandal, Mater. Sci. Semicond. Process. **107**, 104828 (2020). https://doi.org/10.1016/j.mssp.2019.104828
45. A. Umar, R. Kumar, G. Kumar, H. Algarni, S.H. Kim, J. Alloys Compd. **648**, 46 (2015). https://doi.org/10.1016/j.jallcom.2015.04.236
46. J. McGinty, N. Yazdanpanah, C. Price, J.H. ter Horst, J. Sefcik, *The Handbook of Continuous Crystallization*, ed. by B.N. Yazdanpanah (Z. K. Nagy (The Royal Society of Chemistry, London, 2020), p. 50
47. A. Varma, A.S. Mukasyan, A.S. Rogachev, K.V. Manukyan, Chem. Rev. **116**, 14493 (2016). https://doi.org/10.1021/acs.chemrev.6b00279
48. W. Wen, J.M. Wu, RSC Adv. **4**, 58090 (2014). https://doi.org/10.1039/C4RA10145F
49. W. Wen, J.M. Wu, Y.D. Wang, Sens. Actuators B Chem. **184**, 78 (2013). https://doi.org/10.1016/j.snb.2013.04.052
50. M. Guzman, B.M. Flores, L. Malet, S. Godet, Sci. Forum. **916**, 232 (2018). https://doi.org/10.4028/www.scientific.net/MSF.916.232
51. M.J. Chithra, M. Sathya, K. Pushpanathan, Acta Metall. Sin. (Engl Lett). **28**, 394 (2015). https://doi.org/10.1007/s40195-015-0218-8
52. S. Kumar, A. Thakur, V.S. Rangra, S. Sharma, Arab. J. Sci. Eng. **41**, 2393 (2016). https://doi.org/10.1007/s13369-015-1852-1
53. M. Anbuvannan, M. Ramesh, G. Viruthagiri, N. Shanmugam, N. Kannadasan, Synthesis, Spectrochim Acta Mol. Biomol. Spectrosc. **143**, 304 (2015). https://doi.org/10.1016/j.saa.2015.01.124
54. B. Manikandan, T. Endo, S. Kaneko, K.R. Murali, R. John, J. Mater. Sci. Mater. Electron. **29**, 9474 (2018). https://doi.org/10.1007/s10854-018-8981-8
55. K.G. Akpomie, S. Ghosh, M. Gryzenhout, J. Conradie, Sci. Rep. **11**, 8305 (2021). https://doi.org/10.1038/s41598-021-87819-2
56. D. Rajesh, B.V. Lakshmi, C.S. Sunandana, Phys. B Condens. Matter. **407**, 4537 (2012). https://doi.org/10.1016/j.physb.2012.07.050
57. S. Kumar, P.D. Sahare, Opt. Commun. **285**, 5210 (2012). https://doi.org/10.1016/j.optcom.2012.07.125
58. V. Srivastava, D. Gusain, Y.C. Sharma, Ceram. Int. **39**, 9803 (2013). https://doi.org/10.1016/j.ceramint.2013.04.110
59. Y. Khan, S.K. Durrani, M. Mehmood, J. Ahmad, M.R. Khan, S. Firdous, Appl. Surf. Sci. **257**, 1756 (2010). https://doi.org/10.1016/j.apsusc.2010.09.011
60. J. Duraimurugan, G.S. Kumar, M.V.P. Maadeswaran, J. Mater. Sci. Mater. Electron. **29**, 9399 (2018). https://doi.org/10.1007/s10854-018-8964-9
61. M.A. Gondal, Q.A. Drmosh, Z.H. Yamani, T.A. Saleh, Appl. Surf. Sci. **256**, 298 (2009). https://doi.org/10.1016/j.apsusc.2009.08.019
62. Z.N. Kayani, F. Saleemi, I. Batool, Appl. Phys. A **119**, 713 (2015). https://doi.org/10.1007/s00339-015-9019-1
63. M. Gu, L. Hao, Y. Wang, X. Li, Y. Chen, W. Li, L. Jiang, Chem. Phys. **534**, 110750 (2020). https://doi.org/10.1016/j.chemphys.2020.110750
64. M. Sathya, K. Pushpanathan, Appl. Surf. Sci. **449**, 346 (2018). https://doi.org/10.1016/j.apsusc.2017.11.127
65. K.S. Babu, A.R. Reddy, C. Sujatha, K.V. Reddy, A.N.S. Mallika, J. Adv. Ceram. **2**, 260 (2013). https://doi.org/10.1007/s40145-013-0069-6
66. A. Becheri, M. Dürr, P. Lo Nostro, P. Baglioni, J. Nanopart. Res. **10**, 679 (2008). https://doi.org/10.1007/s11051-007-9318-3
67. S. Zandi, P. Kamelin, H. Salamati, H. Ahmadvand, M. Hakimi, Phys. B: Condens. Matter. **406**, 3215 (2011). https://doi.org/10.1016/j.physb.2011.05.026
68. N. Goswami, D.K. Sharma, P.E. Low-Dimensi, Syst. Nanostruct. **42**, 1675 (2010). https://doi.org/10.1016/j.physe.2010.01.023
69. H.M. Rietveld, J. Appl. Crystallogr. **2**, 65 (1969). https://doi.org/10.1107/S0021889869006558
70. B.H. Toby, Power Diffraction. **21**, 67 (2006). https://doi.org/10.1154/1.2179804
71. W.I.F. David, J. Res. Natl. Inst. Stand. Technol. **109**, 107 (2004). https://doi.org/10.6028/jres.109.008
72. N. Khlif, N. Ihzaz, S. Mrabet, A. Alyamani, L.E. Mir, J. Lumin. **245**, 118770 (2022). https://doi.org/10.1016/j.jlumin.2022.118770
73. S.B. Mullani, A.G. Dhodamani, A. Shellikeri, N.B. Mullani, A.K. Tawade, S.N. Tayade, J. Biscay, L. Dennany, S.D. Delekar, Sci. Rep. **10**, 15955 (2020). https://doi.org/10.1038/s41598-020-72756-3
74. S. Barman, S. Sikdar, A. Biswas, B.K. Mandal, R. Das, AIP Conf. Proc. 2220, 020121 (2020) https://doi.org/10.1063/5.0002025
75. A.J. Reddy, M.K. Kokila, H. Nagabhushana, J.L. Rao, C. Shivakumara, B.M. Nagabhushana, R.P.S. Chakradhar, Spectrochim Acta Mol. Biomol. Spectrosc. **81**, 53 (2011). https://doi.org/10.1016/j.saa.2011.05.043
76. A.H. Moharram, S.A. Mansour, M.A. Hussein, M. Rashad, J. Nanomater. 2014, 1 (2014) https://doi.org/10.1155/2014/716210
77. B.D. Cullity, S.R. Stock, *Elements of X-ray Diffraction*, 3rd edn. (Prentice Hall, New Jersey, 2014), pp. 451–518
78. P. Bindu, S. Thomas, J. Theor, Appl. Phys. **8**, 123 (2014). https://doi.org/10.1007/s40094-014-0141-9
79. A. Sharma, V.N. Rai, S. Mani, S. Chawade, Mater. Today: Proc. 26, 58 (2020) https://doi.org/10.1016/j.matpr.2019.05.377
80. F.B. Dejene, J. Phys. Commun. **6**, 075011 (2022). https://doi.org/10.1088/2399-6528/ac8049
81. Y.P. Du, Y.W. Zhang, L.D. Sun, C.H. Yan, J. Phys. Chem. C **112**, 12234 (2008). https://doi.org/10.1021/jp802958x
82. M.J. Chinthra, M. Sathya, K. Pushpanathan, Acta Metall. Sin. (Engl Lett). **28**, 394 (2015). https://doi.org/10.1007/s40195-015-0218-8
83. H.S. Wasly, M.S. Abd ElSadek, M. Henini, Appl. Phys. A **124**, 76 (2018). https://doi.org/10.1007/s00339-017-1482-4
84. R.O. Yathisha, Y.A. Nayaka, Inorg. Chem. Commun. **15**, 107877 (2020). https://doi.org/10.1016/j.inoche.2020.107877
85. H. Morkoç, U. Özgur, *Zinc Oxide: Fundamentals, Materials and Device Technology* (WILEY-VCH Verlag GmbH & Co. KGaA, Weinheim, 2009), p. 477. https://doi.org/10.1002/9783527623945
86. W. Qin, J.A. Szpunar, Philos. Mag Lett. **85**, 649 (2005). https://doi.org/10.1080/09500830500474339
87. A. Kalita, M.P.C. Kalita, Mater. Charact. **137**, 109 (2018). https://doi.org/10.1016/j.matchar.2018.01.013
88. K.V. Gurav, U.M. Patil, S.M. Pawar, J.H. Kim, C.D. Lokhande, J. Alloys Compd. **509**, 7723 (2011). https://doi.org/10.1016/j.jallcom.2011.04.094
89. L. Wolski, J.E. Whitten, I. Sobczak, M. Ziolek, Mater. Res. Bull. **85**, 35 (2017). https://doi.org/10.1016/j.materresbull.2016.08.027

90. T. Ivanova, A. Harizanova, T. Koutzarova, B. Vertruyen, R. Closset, Mater. **15**, 8883 (2022). https://doi.org/10.3390/ma15248883
91. R. Yogamalar, R. Srinivasan, A. Vinu, K. Ariga, A.C. Bose, Solid State Commun. 149, 1919 (2009) https://doi.org/10.1016/j.ssc.2009.07.043
92. H.S. Wasly, M.S. Abd El-Sadek, K.M. Batoo, Mater. Res. Express. **6**, 055003 (2019). https://doi.org/10.1088/2053-1591/ab00ab
93. A.S. Hassanien, A.A. Akl, A.H. Sáaedi, CrystEngComm. **20**, 1716 (2018). https://doi.org/10.1039/C7CE02173A
94. S. Dolabella, A. Borzì, A. Dommann, A. Neels, Small. **6**, 2100932 (2022). https://doi.org/10.1002/smtd.202100932
95. P. Narin, E. Kutlu-Narin, S. Kayral, R. Tulek, S. Gokden, A. Teke, S.B. Lisesivdin, J. Lumin. **251**, 119158 (2022). https://doi.org/10.1016/j.jlumin.2022.119158
96. F. Pola-Albores, F. Paraguay-Delgado, W. Antúnez-Flores, P. Amézaga-Madrid, E. Ríos-Valdovinos, M. Miki-Yoshida, J Nanomater. 2011, 643126 (2011) https://doi.org/10.1155/2011/643126
97. H.E. Okur, N. Bulut, T. Ates, O. Kaygili, (2019) Bull. Mater. Sci. 42, 199 (2019) https://doi.org/10.1007/s12034-019-1877-2
98. S. Krobthong, T. Rungsawang, S. Wongrerkdee, Toxics. **11**, 266 (2023). https://doi.org/10.3390/toxics11030266
99. T.K. Pathak, H.C. Swart, *Zinc Oxide Based Nano Materials and Devices*, ed. by A.M. By, Nahhas (IntechOpen, London, 2019), p. 10. https://doi.org/10.5772/intechopen.78819
100. P.K. Samanta, A. Saha, T. Kamilya, Optik. **126**, 1740 (2015). https://doi.org/10.1016/j.ijleo.2015.04.025
101. E.Y. Shaba, J.O. Jacob, J.O. Tijani, Appl. Water Sci. **11**, 48 (2021). https://doi.org/10.1007/s13201-021-01370-z
102. O. Thoda, G. Xanthopoulou, G. Vekinis, A. Chroneos, Adv. Eng. Mater. **20**, 1800047 (2018). https://doi.org/10.1002/adem.201800047
103. K.V. Manukyan, A. Cross, S. Roslyakov, S. Rouvimov, A.S. Rogachev, E.E. Wolf, A.S. Mukasyan, J. Phys. Chem. C **117**, 24417 (2013). https://doi.org/10.1021/jp408260m
104. M.A. Ali, M.R. Idris, M.E. Quayum, J. Nanostructure Chem. **3**, 36 (2013). https://doi.org/10.1186/2193-8865-3-36
105. S. Agarwal, L.K. Jangir, K.S. Rathore, M. Kumar, K. Awasthi, Appl. Phys. A **125**, 553 (2019). https://doi.org/10.1007/s00339-019-2852-x
106. K. Manjunath, T.N. Ravishankar, D. Kumar, K.P. Priyanka, T. Varghese, H.R. Naika, H. Nagabhushana, S.C. Sharma, J. Dupont, T. Ramakrishnappa, G. Nagaraju, Mater. Res. Bull. **57**, 325 (2014). https://doi.org/10.1016/j.materresbull.2014.06.010
107. J. Josun, P. Sharma, V.K. Garg, Results Opt. **14**, 100601 (2024). https://doi.org/10.1016/j.rio.2023.100601
108. S. Thambidurai, P. Gowthaman, M. Venkatachalam, S. Suresh, J. Alloys Compd. **830**, 154642 (2020). https://doi.org/10.1016/j.jallcom.2020.154642
109. S. Sakohara, M. Ishida, M.A. Anderson, J. Phys. Chem. B **102**, 10169 (1998). https://doi.org/10.1021/jp982594m
110. K. Davis, R. Yarbrough, M. Froeschle, J. White, H. Rathnayake, RSC Adv. **9**, 14638 (2019). https://doi.org/10.1039/C9RA02091H
111. S.S. Kumara, V.R. Rao, G.N. Rao, Mater. Today: Proc. 62, 5494 (2022) https://doi.org/10.1016/j.matpr.2022.04.220
112. W. Zheng, R. Ding, X. Yan, G. He, Mater. Lett. **201**, 85 (2017). https://doi.org/10.1016/j.matlet.2017.04.133
113. A.A. Firooz, R.A. Mirzaie, F. Kamrani, J. Struct. Chem. **59**, 739 (2018). https://doi.org/10.1134/S002247661803037X